A Temperature Window for Chemical Vapor Decomposition Growth of Single-Wall Carbon Nanotubes

G. L. Hornyak, L. Grigorian,[†] **A. C. Dillon, P. A. Parilla, K. M. Jones, and M. J. Heben***

National Renewable Energy Laboratory, 1617 Cole Blvd, Golden, Colorado 80401

Received: October 4, 2001; In Final Form: December 11, 2001

Carbon single-wall nanotubes (SWNTs) grow efficiently from methane on alumina-supported metal catalysts within a fairly narrow temperature window from 680 to 850 °C. An abrupt onset in SWNT growth occurs at the low temperature side of the window, and SWNTs produced at these lower temperatures appear to be relatively free of amorphous or nanocrystalline carbon impurities. Raman spectroscopy shows that SWNT yield drops dramatically at the high-temperature side of the window where most previous chemical vapor decomposition (CVD) studies have been performed. The turn-on at the low-temperature side appears to be controlled by the thermodynamics of SWNT growth, while the turn-off at high temperatures is associated with competitive deposition of amorphous and nanocrystalline carbon. The existence of a temperature window for SWNT growth has not been reported elsewhere, and has important general consequences for CVD growth of SWNTs.

Introduction

Carbon single-wall nanotubes (SWNTs) are exciting new materials with novel physical and chemical properties that should find uses in a variety of technological applications.[1–3] These materials have been synthesized by a variety of techniques including electric-arc discharge,[4,5] laser vaporization,[6] and chemical vapor decomposition (CVD).[7] SWNT growth was first achieved with the electric-arc technique, but control of the growth zone conditions is difficult by this process and, as a result, arc-grown materials tend to be highly impure. More recently, laser-based synthesis has led to the production of high purity materials,[8,9] but high equipment costs and low production rates will probably limit this technique to basic research studies. Both arc- and laser-based production processes typically operate in a batch mode and are therefore poorly suited to high-volume, low cost production. In contrast, the decomposition of carbon-containing gases on supported metal catalysts, i.e., CVD, offers a route by which SWNTs might be continuously and inexpensively produced.

Multiwalled nanotubes and graphitic nanofibers have been grown by CVD for quite some time,[10–13] but the approach has only recently been adapted for SWNT growth. In each case, the growth of the condensed carbon phase is mediated by the catalytic particle. Steps include (1) absorption of the gaseous carbon-containing molecule, (2) dissociation of the molecule to generate carbon atoms, and (3) organization of these atoms into condensed phases. The carbon atoms diffuse either on the surface or through the bulk of the metal particles. The condensed phase is formed by precipitation if the metal particle is supersaturated with dissolved carbon, or by knitting surface carbon atoms into carbonaceous nuclei or preexisting, low energy structures. SWNTs result when the metal particles are small, and appropriate catalysts, gases, and temperatures are employed. SWNTs are currently grown by CVD from meth-

ane,[14–18] carbon monoxide,[7,19] and other hydrocarbons such as benzene,[20] acetylene,[21] or ethylene.[22] Catalysts are typically supported on Al$_2$O$_3$, SiO$_2$, or MgO and consist of metals such as Co, Ni, Fe, and Mo, their oxides, as well as mixtures of these.

All SWNT CVD employing methane has been done at temperatures in the range of 850–1000 °C,[15–18,23] and only a few reports exist for syntheses at lower temperature using C$_2$H$_4$,[22] CO,[19] and (C$_3$H$_7$)$_3$N.[24] Here, we report that methane can be decomposed to form predominantly SWNTs at temperatures as low as 675 °C when certain catalysts are employed. More importantly, the onset of growth with increasing temperature is quite abrupt with some catalysts, such that variations of less than 1 °C can fully activate SWNT growth. Very little amorphous or nanocrystalline carbon is deposited just above the onset temperature despite pronounced SWNT growth. The growth rate is relatively constant as temperature is increased ~125 °C above the onset, but decreases above 800 °C as the deposition of amorphous and nanocrystalline carbon becomes dominant. Together, the onset of growth at low temperatures and the reduction in growth at higher temperatures define a previously unobserved growth window. The window begins at temperatures lower than those investigated elsewhere and ends due to the competitive formation of amorphous/nanocrystalline carbon. As noted earlier, all previous CVD investigations using methane employed temperatures higher than the high-temperature limit of the window reported here. The occurrence of a window for optimal CVD growth offers the possibility to discriminate against the formation of non-SWNT carbon impurities, and low-temperature growth offers energy savings during synthesis. Furthermore, key features of the growth mechanism are revealed since conditions closer to thermal equilibrium are employed. We report on the growth of SWNTs by CVD as a function of temperature and methane partial pressure using Raman spectroscopy, weight-gain measurements, and transmission electron microscopy (TEM). Although the scope of the work presented here is restricted to methane CVD processes, important general conclusions should be applicable to other gases.

* To whom correspondence should be addressed. E-mail: mikeh@nrel.gov.
† Honda R&D Americas, Inc., Fundamental Research Lab, 1381 Kinnear Road, Columbus, OH 43212.
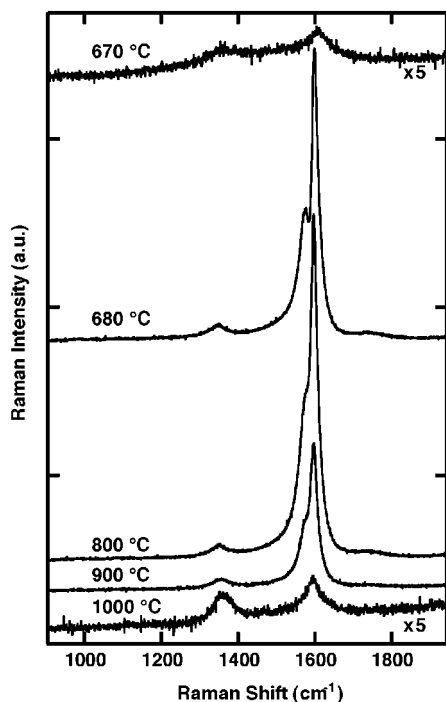
Figure 1. Raman spectra from samples grown by CVD with 40 sccm methane flow at the designated temperatures. Spectra were obtained with 7 mW of 488 nm excitation.

Experimental Section

Metallic catalysts were dispersed onto an alumina support by a technique similar to the one described in ref 15, except that $(C_2H_5)_3SiO_4$ was not employed. The majority of this work (except where noted) was performed with an Fe:Mo catalyst prepared by stirring $Fe_2(SO_4)_3 \cdot 5H_2O$ (97%, Aldrich), $(NH_4)_6$-$Mo_7O_{24} \cdot 4H_2O$ (99.98%, Aldrich), and Al_2O_3 (Degussa, Type C, 85−115 m^2/gm) in deionized water at 80 °C for 1 h, ultrasonicating the mixture for 3 h, and then drying overnight under N_2 in an oven at 100 °C. The dried material was ground and calcined in air at 900 °C for 10 min, allowed to cool, and re-ground. The amounts of starting materials were chosen to produce 2.7 mg of metal in a 6:1 Fe:Mo molar ratio on the ∼ 50 mg of support which was employed in each run. The supported catalyst was placed in a quartz boat in the center of a 1 in. i.d. quartz tube, and CVD was performed at temperatures between 600 and 1000 °C. The CH_4 source gas (ca. 99.99% pure) was introduced at either 10, 40, or 160 sccm and diluted with Ar to a total flow rate of 440 sccm. The pressure was maintained at 600 Torr by feedback control of an exhaust valve, and the CVD time was restricted to 1 h in order to observe the early stages of growth without mass transport limitations. At the conclusion of each run, the methane flow was stopped, and the system was allowed to cool to room temperature under a flow of argon. Raman spectroscopy was performed using 7 mW of the 488 nm line of an Ar ion laser at a resolution of ∼0.6 nm (2−6 cm^{-1}) across the entire range of interest. Calibration was performed with Oriel spectral lamps.

Results and Discussion

Figure 1 shows Raman spectra in the range of 1000 to 1800 cm^{-1} for materials grown with a CH_4 flow rate of 40 sccm at growth temperatures (T_g) between 670 and 1000 °C. The Raman spectrum from a light-gray deposit formed at 670 °C shows a broad, weak feature at 1353 cm^{-1}, the so-called "D-band",[25] which is related to structural disorder of sp^2 bonded nanocrys-

talline and/or amorphous carbon species, and a feature at 1606 cm^{-1} which is related to the fundamental E_{2g} mode of graphite.[26] There is no evidence for the presence of SWNTs, and the data shows that only poorly organized carbon is formed at $T_g = 670$ °C. The total weight increase for this sample was ∼3% relative to the initial sample weight. The Raman spectra for deposits grown at 650 °C (not shown) were virtually identical, and there was no carbon deposition for $T_g < 650$ °C.

When T_g was increased by only two °C to 672 °C, a dark-black deposit formed on the upstream portion of the catalyst/ support, while the downstream portion was light-gray as was found at 670 °C. Raman spectroscopy of the dark-black regions revealed the well-known sharp feature at 1593 cm^{-1}, with a shoulder at 1567 cm^{-1}, as expected for scattering from resonantly enhanced SWNTs.[27] This temperature is apparently very close to the absolute lower limit for SWNT formation under these conditions. The entire catalyst/support became covered with a uniformly black deposit at $T_g = 680$ °C, and the sample weight was increased by ∼25%. The weight gain was accompanied by the appearance of strong SWNT modes in the Raman spectrum, and even stronger signals were seen from samples grown at 700 and 800 °C (Figure 1). However, the intensity was reduced at $T_g = 900$ °C, and the SWNT bands disappeared almost completely at $T_g = 1000$ °C (Figure 1). The Raman spectrum from the 1000 °C sample was quite similar to the spectrum from the 670 °C sample except that the two bands are slightly more intense and narrow. The growth in the D-band is consistent with the deposition of more amorphous and nanocrystalline carbon, while the additional sharpness near 1590 cm^{-1} is due to the presence of a small number of SWNTs (Figure 2b).

The Raman data of Figure 1 shows that SWNTs grow efficiently within a fairly narrow T_g range from ∼680 to ∼850 °C. There is very little or no carbon deposition at lower temperatures, and the deposit is predominantly in the form of amorphous and/or nanocrystalline carbon at higher temperatures. These conclusions are supported by numerous TEM images taken from samples deposited over a wide range of temperatures. For example, Figure 2a,b show representative TEM images of samples grown at 700 and 1000 °C, respectively. The samples were lightly sonicated in 1 M HF to remove the Al_2O_3 support. The image of Figure 2a shows mostly SWNT ropes, while Figure 2b shows predominantly amorphous carbon and nanocrystalline graphite, and a very few SWNTs.

The growth temperature window for SWNTs is seen more clearly in Figure 3a where the intensity of the major SWNT tangential Raman mode is plotted as a function of temperature for the three different CH_4 flow rates. In each case, the intensity of the SWNT mode near 1593 cm^{-1} is observed to increase from approximately zero (i.e. no greater than the intensity of the D-band signal) to a maximum value for the window over a very narrow increase in temperature. The data taken at 10 sccm is most striking with an increase of temperature of only 10 °C giving rise to strong SWNT growth. At CH_4 flow rates of 40 and 160 sccm, temperature increases of 30 and 20 °C, respectively, are required to fully turn on SWNT growth on the low-temperature side of the window. For all CH_4 flow rates, the intensity of the major Raman feature remains high as the growth temperature is increased above the low temperature onset, but declines to nearly zero again between 800 and 1000 °C.

Figure 3b shows the weight gained due to carbon deposition as a function of T_g for the three different CH_4 flow rates. All curves show a sharp onset in weight gain beginning below 700

Letters

J. Phys. Chem. B, Vol. 106, No. 11, 2002 **2823**
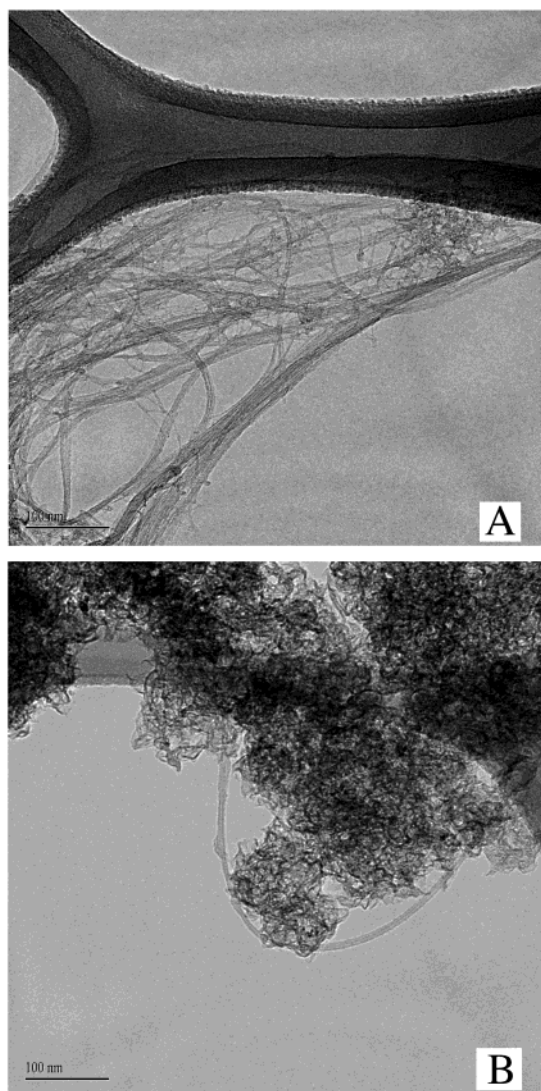
Figure 2. Transmission electron microscope images of SWNTs formed under (a) 700 °C and (b) 1000 °C temperatures and 40 sccm methane. Both samples were prepared by gentle sonication in 1 M hydrofluoric acid at 80 °C to remove the Al_2O_3 support.

Figure 3. (a) The intensity of the major Raman SWNT tangential mode near 1593 cm^{-1} plotted against CVD temperature. A window for optimized SWNT growth is shown for three methane flow rates (10, 40 and 160 sccm). (b) The percent weight gained, relative to the initial catalyst/support weight, after CVD plotted against temperature. The curves for three methane flow rates (10, 40, and 160 sccm) are shown. The weight-gain curve for bare alumina at 40 sccm is also shown.

°C, a plateau spanning from 700 to 800 °C, a local minimum between 800 and 950 °C, and an increase in weight as T_g is increased to 1000 °C. Since the total gas flow rate was held constant at 440 sccm, an increased CH_4 flow rate corresponds to an increased CH_4 partial pressure as well as an increased driving force for CH_4 decomposition. Thus, one might expect the carbon deposition to begin at the lowest temperatures for the 160 sccm experiments. Consistently, the 160 sccm flow rate data shows weight gain at a temperature as low as 660 °C (Figure 3b). However, despite showing no weight gain until 670 °C, the turn-on in SWNT growth is much more abrupt at 40 sccm (Figure 3a). Consequently, the plateau in weight gain (Figure 3b) is reached at a lower temperature than observed in the 160 sccm data. The onset of SWNT growth occurs 30 °C higher in the 10 sccm case, but is quite abrupt (Figure 3a). The data can be reconciled by considering that only SWNTs grow at the low temperatures with the lower driving force for CH_4 decomposition associated with the 10 and 40 sccm flow rates, while both SWNT and non-SWNT carbonaceous solids are formed in parallel at 160 sccm. The concomitant deposition of amorphous/nanocrystalline carbon at the highest methane partial pressures deactivates some catalytic particles thereby precluding some SWNT growth. Note that the intensity of the tangential

Raman band is ~ 40% lower for the 160 sccm samples as compared to the 10 and 40 sccm samples (Figure 3a). This demonstrates that CH_4 partial pressure is an important parameter for optimizing CVD growth of SWNTs.

The intensity of the SWNT Raman mode at 1593 cm^{-1} is maximized to approximately the same value within the plateau for both the 10 and 40 sccm flow rates (Figure 3a). Similar weight gains (~30%) are also observed at the plateau values for these two flow rates (Figure 3b). Consequently, it is reasonable to conclude that the same amount of SWNTs are made in the two cases, and that SWNTs are the predominant product as confirmed by TEM. Furthermore, since the amount of SWNT growth is independent of flow rate, we can also conclude that the growth rate in the plateau region is controlled by the SWNT growth reactions on the catalyst particles rather than by limitations associated with CH_4 transport to the metal catalysts. This finding appears to be in contradiction to the work of Hafner et al.[22] wherein the growth of SWNTs was made dominant by limiting the supply of carbon to the catalyst particles.

The weight-gain curve for a control Al_2O_3 sample shows very little carbon deposition at low temperatures and a strongly
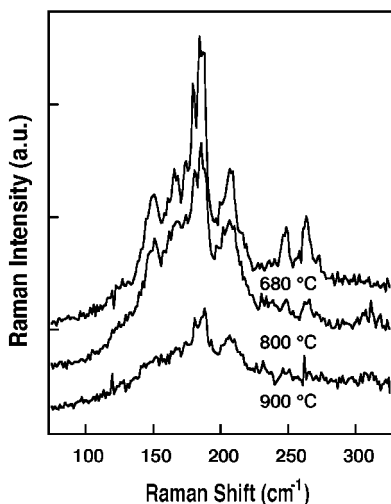
Figure 4. Raman spectra in the region of the radial breathing modes for materials grown under 40 sccm methane flow at 680, 800, and 900 °C.

increasing weight gain with increasing temperatures above 900 °C (Figure 3b). Here, the support material was processed through the same steps which produced SWNTs except that catalytic metals were omitted. The amount of uncatalyzed deposition increased dramatically at higher temperatures such that the weight of the supported catalyst was doubled over the course of the 1 h deposition at 1000 °C. The weight gain of the Fe: Mo-decorated Al_2O_3 at 1000 °C and the same flow rate (40 sccm) is ~36% less than for the control sample. Thus it seems that the Fe:Mo-decorated Al_2O_3 support possesses either a reduced surface area in comparison to the control Al_2O_3, or a surface chemistry which is altered by processing such that the decomposition of methane is suppressed. In either case, it is apparent that the increased weight gain at the higher temperatures is due to deposition of non-SWNT carbon. Note that the mass gain at high temperatures becomes a function of the methane flow rate for the metal-decorated samples as expected for a mass transport-limited deposition mechanism.

Collectively, the data in Figure 3 indicate that SWNT growth occurs in parallel with the deposition of nanocrystalline and amorphous carbon. In general, there is a temperature window in which SWNT growth proceeds on the catalytic metal particles, as well as a background carbon deposition reaction which occurs predominantly on the support and increases strongly with both temperature and CH_4 flow rate. The two parallel pathways for the decomposition of CH_4 into the SWNT and non-SWNT solids have very different temperature dependencies with the catalysts employed here, so the competing pathways can be observed. We speculate that the deposition rates for SWNT and non-SWNT carbons become approximately equal near the minimum in the weight-gain curves (Figure 3b). The SWNT growth pathway predominates at the lower temperatures, and the non-SWNT pathway is dominant at high temperature. The two competing pathways are better separated in temperature at the lower CH_4 partial pressures, and the local minima in the weight-gain curves shift to higher temperature with decreasing CH_4 flow rate.

Figure 4 shows the Raman spectra in the region of the radial breathing modes for materials grown at a CH_4 flow rate of 40 sccm. Only the data for growth at 680, 800, and 900 °C are displayed since these were the only samples to show strong radial breathing modes, consistent with the strong tangential signals in Figure 1. At first glance the 680 °C spectrum may be interpreted as being noisy, but virtually all of the features are

reproduced in the spectrum from the 800 °C sample. Thus we can conclude that many different types of tubes are present. Only the most intense radial breathing modes are observed from the sample grown at 900 °C, but it is evident that the overall tube distribution is not greatly altered. It is therefore apparent that the size distribution of SWNTs is not significantly affected by changes in growth temperature. Thus, a set of tubes begin to grow with this specific catalyst composition once temperatures exceed the low-temperature onset, and this same set grows at higher temperatures if growth is not prohibited or preempted by the deposition of other condensed carbon phases.

The spectrum from the material grown at 680 °C shows the presence of over a dozen radial breathing modes (Figure 4) representing SWNTs ranging in diameter from ~1.5 to 0.8 nm.[27] It is probable that many other tubes are also present but simply not observed due to lack of resonance with the 488 nm Raman excitation. Even though the SWNT signals in Figure 1 are quite intense for T_g = 680 to 800 °C, requiring only 90 s for acquisition, the A_{1g}, E_{1g}, and E_{2g} modes that comprise the major Raman features in the region of 1570−1590 cm^{-1} are poorly resolved. In comparison, the SWNT modes at 1593 and 1567 cm^{-1} are much better separated in laser-generated materials.[9] Therefore, we believe that the lack of resolution in the main SWNT signal is due to the polydispersity in diameter[28] for the tubes produced via this CVD method. However, note that the degree of resolution in Figure 1 is highest for samples made at the lowest growth temperatures. Under these conditions we expect a minimum of amorphous or nanocrystalline carbon deposition that might also obscure the individual SWNT modes.

We have observed the same general behavior of an abrupt onset in SWNT growth at a low temperature limit with several other catalyst formulations. Of particular interest was an Fe/Co/Mo composition formed in a 12:3:2 molar ratio. In this case we observed the onset of SWNT growth to be slightly higher at 685 °C, but the growth could be fully activated or deactivated by changes in temperature that were smaller than our experimental resolution (± 1 °C). The growth persisted over a temperature plateau, and then decreased as the deposition of non-SWNT carbons dominated at higher temperatures. Also of note was the case of pure Fe. Here, SWNTs did not begin to grow until temperatures exceeded 750 °C. The onset of growth was not abrupt, and the weight gain and Raman signals increased so slowly with temperature that the competing pathways of SWNT and non-SWNT deposition could not be readily discerned as a minimum in the weight-gain curve.

Summary and Conclusions

Our observation that SWNTs grow abruptly with increasing temperature suggests that the growth is turned-on by thermodynamic considerations. SWNTs have been predicted to be more stable than graphitic strips of width corresponding to the tube circumference when the tube diameter is greater than 0.4−0.6 nm.[29,30] However, these calculations were based on comparisons of a fixed, large number of atoms and do not directly comment on the relative stability of fullerene hemispheres, single or multilayer graphene disks, and nanoscale amorphous carbon structures having a small number of atoms. As proposed in the yarmulke mechanism[7] and supported recently by theory,[31] the hemispherical nuclei for SWNT growth could be more thermodynamically stable than single-layer graphene disks of the same number of atoms simply because the ratio of edge atoms to "bulk" (i.e., fully bonded) atoms would be lower in the hemisphere. According to this simple view, a transition from SWNT to non-SWNT growth would occur when the density of

Letters

J. Phys. Chem. B, Vol. 106, No. 11, 2002 **2825**

carbon atoms precipitated from the carbon-saturated metal particles exceeded some critical density such that non-SWNT nuclei became more stable. According to Hafner et al.,[22] such a transition is observed when the carbon precipitation reaction is limited by supply of the carbon containing gas to the particle rather than by diffusion within the catalytic particle. In our work, we observe the preferential formation of SWNT when the driving force for methane decomposition is limited at low growth temperatures and low methane partial pressures.

Regardless of the fundamental reasons for the formation of a SWNT nucleus on a catalytic particle, the nucleus is expected to grow very quickly in length with the addition of more carbon atoms. In contrast, CVD growth of nanocrystalline graphite and amorphous carbon would require the formation of new nuclei, and therefore would be kinetically hindered even if favored by thermodynamics. Any kinetic advantage for SWNT growth is eventually overcome as the thermodynamic driving force for formation of amorphous/nanocrystalline carbon increases at the higher temperatures and methane partial pressures. Carbon deposition occurs indiscriminately on the support at still higher temperatures as the reaction proceeds without catalysis.

For the first time, we have demonstrated the existence of a temperature window for the effective growth of SWNTs by CVD, and shown that low temperatures are preferred for the growth of high-density SWNTs using methane. We tentatively conclude that the onset of SWNT growth on metal catalysts at low temperatures can be determined by purely thermodynamic considerations when the growth rate of SWNTs is high and the deposition of amorphous/graphitic carbon is hindered. Catalytic particles capable of growing SWNTs continue to do so until de-activated by the formation of amorphous or nanocrystalline carbon. Deposition of amorphous/graphitic carbon becomes competitive at higher temperatures until SWNT growth is completely quenched.

References and Notes

(1) Ebbesen, T. W. *Phys. Today* **1996**, June, p 26.

(2) Collins, P. G.; Avouris, P. *Sci. Am.* **2000**, Dec, p 62.

(3) Dresselhaus, M. S.; Dresselhaus, G.; Eklund, P. C. *Science of Fullerenes and Carbon Nanotubes*; Academic Press: New York, 1996.

(4) Iijima, S.; Ichihashi, T. *Nature* **1993**, *363*, 603.

(5) Bethune, D. S.; Kiang, C.-H.; de Vries, M. S.; Gorman, G.; Savoy, R.; Vasquez, J.; Beyers, R. *Nature* **1999**, *363*, 605.

(6) Guo. T.; Nikolaev, P.; Thess, A.; Colbert, D. T.; Smalley, R. E. *Chem. Phys. Lett.* **1995**, *243*, 49.

(7) Dai, H.; Rinzler, A. G.; Nikolaev, P.; Thess, A.; Colbert, D. T.; Smalley, R. E. *Chem. Phys. Lett.* **1996**, *260*, 471.

(8) Rinzler, A. G.; Lui, J.; Dai, H.; Nikolaev, P. Huffman, C. B.; Rodriguez-Macias, F. J.; Boul, P. J.; Lu, A. H.; Heymann, D.; Colbert, D. T.; Lee, R. S.; Fischer, J. E.; Rao, A. M.; Eklund, P. C.; Smalley, R. E. *Appl. Phys. A* **1998**, *67*, 29.

(9) Dillon, A. C.; Gennett, T.; Jones, K. M.; Alleman, J. L.; Parilla, P. A.; Heben, M. J. *Adv. Mater.* **1999**, *11*, 1354.

(10) Baker, R. T. K.; Harris, P. S.; Thomas, R. B.; Waite, R. J. *J. Catal.* **1973**, *30*, 86.

(11) Baker, R. T. K.; Harris, P. S. In *Physics and Chemistry of Carbon*; Walker, P. L., Thrower, P. A., Eds.; Marcel Dekker: New York, 1978; Vol 14; p 83.

(12) Tibbets, G. G. *J. Cryst. Growth* **1984**, *66*, 632.

(13) Rodriguez, N. M. *J. Mater. Res.* **1993**, *8*, 3233.

(14) Kong, J.; Cassell, A. M.; Dai, H. *Chem. Phys. Lett.* **1998**, *292*, 567.

(15) Cassell, A. M.; Raymakers, J. A.; Kong, J.; Dai, H. *J. Phys. Chem. B* **1999**, *103*, 6484.

(16) Colomer, J.-F.; Stephan, C.; Lefrant, S.; Van Tendeloo, G.; Willems, I.; Kónya, Z.; Fonseca, A.; Laurent, Ch.; Nagy, J. B. *Chem. Phys. Lett.* **2000**, *317*, 83.

(17) Bacsa, R. R.; Laurent, Ch.; Peigney, A.; Bacsa, W. S.; Vaugien, Th.; Rousset, A. *Chem. Phys. Lett.* **2000**, *323*, 566.

(18) Su, M.; Zheng, B.; Liu, J. *Chem. Phys. Lett.* **2000**, *322*, 321.

(19) Kitiyanan, B.; Alvarez, W. E.; Harwell, J. H.; Resasco, D. E. *Chem. Phys. Lett.* **2000**, *317*, 497.

(20) Ci, L.; Wei, J.; Wei, B.; Liang, J.; Xu, C.; Wu, D. *Carbon* **2001**, *39*, 329.

(21) Bladh, K.; Falk, L. K. L.; Rohmund, F. *Appl. Phys. A* **2000**, *70*, 317.

(22) Hafner, J. H.; Bronikowski, M. J.; Azamian, B. R.; Nikolaev, P.; Rinzler, A. G.; Colbert, D. T.; Smith, K. A.; Smalley, R. E. *Chem. Phys. Lett.* **1998**, *296*, 195.

(23) Flahaut, E.; Govindaraj, A.; Peigney, A.; Laurent, Ch.; Rousset, A.; Rao, C. N. R. *Chem. Phys. Lett.* **1999**, *300*, 236.

(24) Tang, Z. K.; Sun, H. D.; Wang, J.; Chen, J.; Li, G. *Appl. Phys. Lett.* **1998**, *73*, 2287.

(25) Eklund, P. C.; Holden, J. M.; Jishi, R. A. *Carbon* **1995**, *33*, 959.

(26) Holden, J. M.; Zhou, P.; Bi, X.-X.; Eklund, P. C.; Bandow, S.; Jishi, R. A.; Das Chowdhury, K.; Dresselhaus, G.; Dresselhaus, M. S. *Chem. Phys. Lett.* **1994**, *220*, 186.

(27) Rao, A. M.; Richter, E.; Bandow, S.; Chase, B.; Eklund, P. C.; Williams, K. A.; Fang, S.; Subbaswamy, K. R.; Menon, M.; Thess, A.; Smalley, R. E.; Dresselhaus, G.; Dresselhaus, M. S. *Science* **1997**, *275*, 187.

(28) Kasuya, A.; Sasaki, Y.; Saito, Y.; Tohji, K.; Nishina, Y. *Phys. Rev. Lett.* **1997**, *78*, 4434.

(29) Sawada, S.; Hamada, N. *Solid State Commun.* **1992**, *83*, 917.

(30) Lucas, A. A.; Lambin, P. H.; Smalley, R. E. *J. Phys. Chem. Solids* **1993**, *54*, 587.

(31) Sinnott, S. B.; Andrews, R.; Qian, D.; Rao, A. M.; Mao, Z.; Dickey, E. C.; Derbyshire, F. *Chem. Phys. Lett.* **1999**, *315*, 25.